JOURNAL OF MATERIALS SCIENCE 21 (1986) 1956–1962

Recovery in cold-worked alloy under pressure: example of AISI 316 stainless steel

MOHAMMAD YOUSUF, P. Ch. SAHU, V. S. RAGHUNATHAN, K. GOVINDA RAJAN
Indira Gandhi Centre for Atomic Research, Kalpakkam 603 102, Tamil Nadu, India

In this paper, we report the behaviour of defects under high pressure in severely cold-deformed 316 stainless steel. *In situ* electrical resistivity measurements indicate a minimum in the reduced resistivity ratio at 2 GPa associated with a characteristic relaxation time of 500 ± 5 sec. Microhardness data on pressure-treated and recovered samples are consistent with the electrical resistivity behaviour. X-ray powder diffraction rings indicate sharpening beyond 2 GPa. The decrease in the full width at half maximum (FWHM) of the strongest ring is about 2% at pressures beyond 2 GPa. Transmission electron microscopy reveals that samples pressure-treated beyond 2 GPa have a polygonized dislocation structure. This is in sharp contrast to the tangled dislocation structure observed in the cold-worked samples. The experimental results suggest a recovery stage in cold-worked stainless steel at 2 GPa. We propose that the recovery process is activated through an enhanced vacancy concentration caused by deformation, a pressure-induced vacancy–dislocation interaction and consequently a pressure-assisted dislocation mobility leading to polygonization.

1. Introduction

Attention has recently been focused on the recovery stages under hydrostatic pressure in materials after irradiation, quenching and splat quenching from the liquid state. For example, Kulcinski [1] observed that annealing neutron-irradiated molybdenum at high pressure causes the recovery to occur at lower temperatures. Specifically, he observed that at 2 GPa, the Stage III recovery (150° C) is lowered to 90° C, and that at 4 GPa it is lowered to room temperature. Moreover, the temperature for complete lattice parameter recovery is lowered from 800° C at atmospheric pressure to room temperature at 7 GPa. Hydrostatic pressure measurements performed up to 12 GPa on the amorphous alloy $Fe_{40}Ni_{40}P_{14}B_6$ revealed that the two prominent structural relaxation stages occurring at 240 and 350° C (at atmospheric pressure) were lowered to room temperature by application of ~4 and ~6 GPa pressure, respectively [2, 3]. Recent experiments on cold-deformed thorium and uranium indicate that they undergo pressure-induced recovery at 4.5 and 6 GPa, respectively [4, 5]. Here, electrical resistivity is found to be strongly time-dependent at pressures of 4.5 GPa in thorium and 6 GPa in uranium. As the defect recovery is a kinetic process, the appropriate approach is to impart an isochronal–isobaric treatment to the sample and monitor a suitable time-dependent property such as electrical resistivity. This *in situ* measurement should preferably be supplemented by data on microhardness, X-ray diffraction, transmission electron microscopy, etc. on the pressure-treated and recovered samples.

2. Resistivity as a tool to study the recovery process

AISI 316 stainless steel has a number of constituent elements, and obtaining an exact expression for electrical resistivity for this alloy is a very difficult task. However, for the purpose of defect studies, following the practice in the literature, we adopt a qualitative analysis [6–8]. The electrical resistivity of a d-band, polycrystalline, cold-worked alloy ϱ_{CS} can be written as

$$\varrho_{CS} = \varrho_p + \varrho_{s\text{-}d} + \varrho_i + \varrho_V + \varrho_I + \varrho_\perp + \varrho_g \quad (1)$$

Here ϱ_p is the resistivity arising due to the conduction (sp-) electron–phonon scattering. Since the transition metal consists of partially filled d-bands, these act as traps for conduction electrons. This is the origin of s–d scattering and results in a contribution $\varrho_{s\text{-}d}$ in Equation 1. Alloying elements such as cobalt, nickel, phosphorus and silicon will modify the resistivity [9, 10] and this is represented by ϱ_i. ϱ_V, ϱ_I, $\varrho_\perp$ and ϱ_g refer to the resistivity due to the vacancies, interstitials, dislocations and grain boundaries, respectively. In Table I, estimates of the contributions to resistivity by various mechanisms in stainless steel are listed. It is of interest to note that the estimated values are in close agreement with the observed values at room temperature. If the annealing of the sample is performed with minimum recrystallization, then the modified resistivity ϱ can be written as

$$\varrho = \varrho_p + \varrho_{s\text{-}d} + \varrho_i + \varrho_g \quad (2)$$

The difference $\varrho_{CS} - \varrho_{AS} = \Delta\varrho$ (say) is a measure of the defect contribution, and the value for severely cold-worked stainless steel is estimated in Table I.

0022–2461/86 $03.00 + .12

TABLE I Electrical resistivity contribution from different mechanisms*

Mechanism	Value ($\mu\Omega$cm) for metals indicated [6–10]	Estimated value ($\mu\Omega$cm) for 316 stainless steel	Value ($\mu\Omega$cm) for CS used in present work
ϱ_p	2.3 (Fe)	2.0	2.0
ϱ_{s-d}	4.6 (Fe)	4.0	4.0
ϱ_i (Cr)	6.3/at % (Cr in Cu)	1.5/at % (Cr in Fe)	26
ϱ_i (Ni)	1.2/at % (Ni in Cu)	2.5/at % (Ni in Fe)	30
ϱ_i (Mo)	–	1.5/at % (Mo in Fe)	3.75
ϱ_i (Mn)	2.9/at % (Mn in Cu)	2.9/at % (Mn in Fe)	3.9
ϱ_i (Si)	3.95/at % (Si in Cu)	4/at % (C in Fe)	2.72
ϱ_i (C)	3/at % (C in Fe)	3/at % (C in Fe)	0.15
ϱ_i (P)	6.7/at % (P in Cu)	7/at % (P in Fe)	0.33
ϱ_i (S)	–	6/at % (S in Fe)	0.1
ϱ_V	9.0/at % (Fe)	9.0/at % (Fe)	1.5
ϱ_I	15/at % (Cu)	40/at % (Fe)	2.0
$\varrho_\perp$	$2.3 \times 10^{-13} N_d$†	$2.3 \times 10^{-12} N_d$	2.3
ϱ_g	$\lesssim 10^{-3}\varrho_\perp$	$\lesssim 10^{-3}\varrho_\perp$	$\lesssim 0.002$

*(a) It is found that the defect contribution is about 7% and is in close agreement with the experimental value. (b) All values at 300 K. (c) Ideal resistivity of Fe $\varrho_{Fe} = 6.9\,\mu\Omega$cm. (d) Resistivity in annealed stainless steel $\varrho_{AS} = 79.57\,\mu\Omega$cm. (e) Resistivity in cold-worked stainless steel $\varrho_{CS} = 85.37\,\mu\Omega$cm. (f) $\mathscr{R}_{cal} = (\varrho_{CS} - \varrho_{AS})/\varrho_{AS} = 0.0729$ (from (d) and (e)); $\mathscr{R}_{obs} = 0.0710$ (Fig. 3).
†N_d is the number of dislocation lines per unit area [9, 10].

Since pressure will change ϱ_V, ϱ_I and $\varrho_\perp$ mainly by reducing the concentrations of point defects and dislocations (leading to recovery), electrical resistivity could be used as a tool to understand the defect behaviour under pressure.

3. Experimental procedure

The chemical composition (wt %) of the AISI 316 austenitic stainless steel used in this investigation as given by the supplier (Sandvik, Sweden) was 0.05 C, 17.45 Cr, 11.81 Ni, 2.5 Mo, 0.68 Si, 1.35 Mn, 0.011 S, 0.047 P and balance Fe. This alloy was cold-rolled into strips of about 0.06 mm thickness, starting from a thickness of 1.6 mm [11]. A 1 cm × 1 cm foil was ground to 0.015 mm thickness using a jig described previously [12] and samples of 1 mm × 0.5 mm were cut from this ground piece for high-pressure resistivity measurements. Samples obtained in this way are referred to as CS. Similar samples were cut and solution-annealed for one hour at 1080° C and then quenched in water. This sample was again heat-treated at 400° C to anneal out excess point defects. Samples treated this way are termed AS in the subsequent sections. Samples prepared for microhardness tests were 0.07 mm thick and received similar treatment as described above.

A three-sample, four-probe and twelve-lead arrangement, as depicted in Fig. 1, in a Bridgman opposed anvil configuration, was used in the present work. This facilitated the *in situ* calibration of the high-pressure cell. A pressure step of about 500 MPa was imparted and the resistivity variation with respect to time was monitored for a fixed period of 30 min in each case. The pressure-step treatment was imparted up to 12 GPa on the samples and the resistivity monitored. Samples that were pressure-treated at 12 GPa were termed PS.

Pressure was generated by concentrating the load on a pair of maraging steel anvils. The samples were housed in a pyrophyllite container and AgCl served as the pressure transmitter. As the shear strength of AgCl is low ($\sim$ 50 MPa), the pressure on the sample is nearly hydrostatic. Internal calibrants like bismuth or tin were used to monitor the sample pressure [13, 14]. By measuring the width of the bismuth I to II transition at 2.54 GPa, an estimate of the uniaxial stress component was found to be less than 0.5% as shown in Fig. 2. This result is consistent with the findings reported by others [15, 16]. The electrical resistivity in our laboratory can be measured with a sensitivity of 1 in 10^5 and the time resolution is 0.25 sec.

Sample preparation for TEM was done by a jet polishing technique [17]. A mixture of 54% orthophosphoric acid, 36% sulphuric acid and 10% methanol was used as the electrolyte, with the sample as the anode. The bath was maintained at 60° C and the thinning was done by applying about 60 V d.c.

4. Approach to the study of defect behaviour under pressure

In studying the resistivity changes and evaluating the contribution due to defect behaviour, one must eliminate the geometrical deformations due to non-hydrostatic components of pressure. If samples of CS and AS of exactly the same sizes and shapes are made and studied in the high-pressure cell, the effect of geometrical distortion can be reduced. In practice, this is a difficult task, and alternatively the following approach is taken.

If g and R stand for the geometrical factor and the resistance of a sample, then the resistivities of CS and AS are

$$\varrho_{CS} = g_{CS} R_{CS}; \quad \varrho_{AS} = g_{AS} R_{AS} \tag{3}$$

Combining Equations 1, 2 and 3, we have for $\Delta\varrho$ the expression

$$\Delta\varrho = g_{CS} R_{CS} - g_{AS} R_{AS} = \varrho_V + \varrho_I + \varrho_\perp \tag{4}$$

Expressing the resistance in terms of the relevant voltages and currents,

$$\Delta\varrho = \frac{V_{CS}}{I_{CS}} g_{CS} - \frac{V_{AS}}{I_{AS}} g_{AS} = \frac{1}{I}(V_{CS} g_{CS} - V_{AS} g_{AS}) \tag{5}$$

if we chose $I_{CS} = I_{AS} = I$ (say).

Now defining the reduced resistivity ratio $\mathscr{R} = \Delta\varrho/\varrho_{AS}$, we have

$$\mathscr{R} = \left(\frac{V_{CS}}{V_{AS}}\frac{g_{CS}}{g_{AS}} - 1\right) = (\varrho_V + \varrho_I + \varrho_\perp)/(\varrho_p + \varrho_{s-d} + \varrho_i) \tag{6}$$

Standard four-probe resistivity measurements were

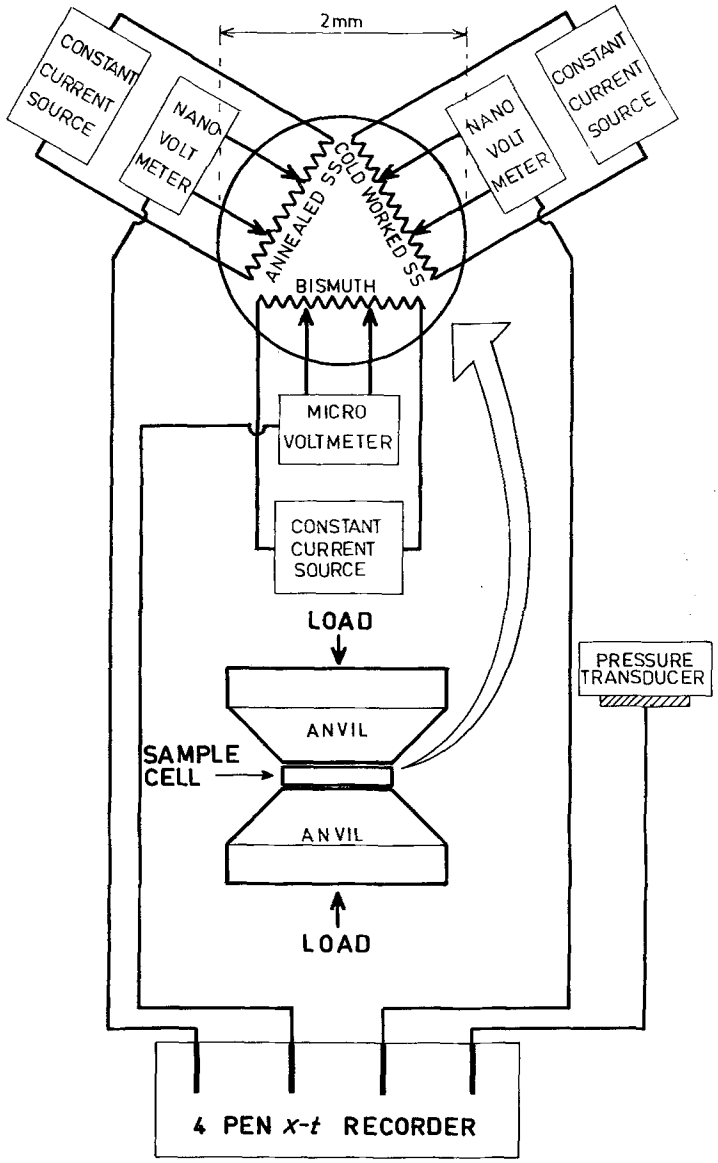

Figure 1 The sample cell is shown in position in an opposed anvil apparatus. The arrangement for the three-sample, four-probe, twelve-lead assembly is depicted separately where annealed stainless steel (AS), cold-worked stainless steel (CS) are shown with bismuth as the pressure marker (internal calibrant). Other features shown in the figure are self-explanatory.

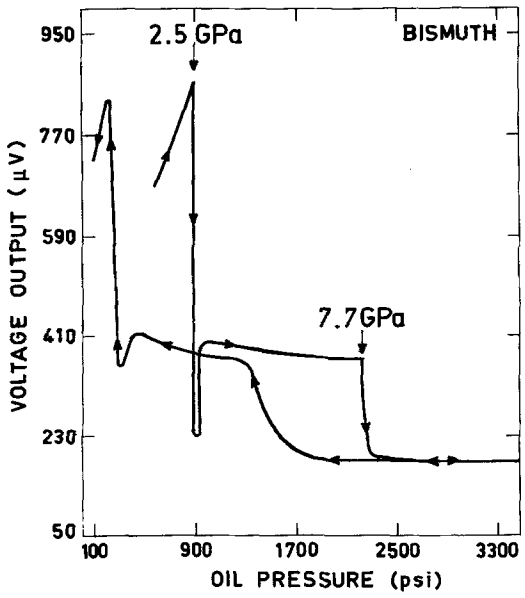

Figure 2 Voltage output from bismuth as a function of oil pressure of the hydraulic press. The two structural phase transitions occurring at 2.5 and 7.7 GPa are marked for the loading run. 1 psi = 6.895 kPa.

carried out on carefully prepared CS and AS samples to yield the quantity $\mathscr{R}$ under ambient conditions. The pressure cell was then loaded, and the voltages V_{CS} and V_{AS} were measured at a pressure close to 100 kPa. Substituting the values of $\mathscr{R}$, V_{CS} and V_{AS}, the quantity g_{CS}/g_{AS} was evaluated. In the subsequent high-pressure measurements, it was assumed that the g factors of both the CS and AS samples were affected in a similar way, and that when V_{CS} and V_{AS} are measured at high pressures, the quantity $[(V_{CS}/V_{AS})(g_{CS}/g_{AS}) - 1]$ will yield the reduced resistivity ratio $\mathscr{R}$.

5. Results

5.1. Steady-state electrical resistivity

A plot of reduced resistivity ratio $\mathscr{R}$ against the sample pressure is shown in Fig. 3. Here ϱ_{CS}, used to evaluate $\mathscr{R}$, pertains to the steady-state value of the resistivity of CS samples. It can be seen from the figure that initially $\mathscr{R}$ decreases sharply with pressure giving $d\mathscr{R}/dp = -(2.15 \pm 0.05) \times 10^{-2}\,GPa^{-1}$. Beyond 2 GPa, $\mathscr{R}$ starts increasing, leading to $d\mathscr{R}/dp = +(2.3 \pm 0.5) \times 10^{-3}\,GPa^{-1}$. Above 5 GPa there is no appreciable change in $d\mathscr{R}/dp$.

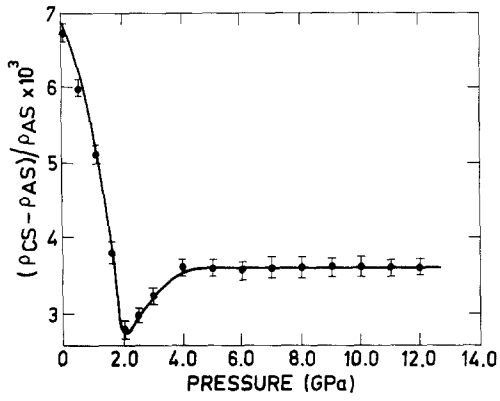

Figure 3 Reduced resistivity ratio plotted as a function of pressure. An initial sharp decrease leads to $d\mathscr{R}/dp = -(2.15 \pm 0.05) \times 10^{-2}\,GPa^{-1}$. However at 2 GPa, a change in the sign of the slope can be seen and beyond 2 GPa $d\mathscr{R}/dp = +(2.3 \pm 0.5) \times 10^{-3}\,GPa^{-1}$. Above 5 GPa $\mathscr{R}$ is almost constant.

5.2. Time-dependent resistivity and kinetics of relaxation

During the pressure-step loading, the electrical resistivity in CS exhibits a strong time dependence. In Fig. 4, typical raw data of the time variation of resistance of the three samples AS, CS and PS are shown. All are recorded at 2 GPa. In the case of CS, the time dependence was a maximum at 2 GPa, beyond which pressure it was weak. The time-dependent resistivity behaviour was analysed to yield a characteristic relaxation time using the relation [9, 10]

$$\mathscr{R}_t^p = \mathscr{R}_0^p + (\mathscr{R}_\infty^p - \mathscr{R}_0^p)\left[1 - \exp\left(-\frac{t}{\tau^p}\right)\right] \quad (7)$$

where superscript p stands for the prevailing pressure at which Equation 7 is used, $\mathscr{R}_t^p$ is the reduced resistivity ratio at any instant of time t, $\mathscr{R}_0^p$ and $\mathscr{R}_\infty^p$ are the initial and steady-state reduced resistivity ratios, and τ^p is the relevant relaxation time. This relation, when used to analyse the experimental results, was found to yield consistent values of τ^p (within ± 5 sec). Fig. 5 shows the variation of the relaxation time as a function of pressure for a CS sample, and it is observed that the maximum value of τ^p is ~ 500 sec at 2 GPa.

5.3. Microhardness measurements

Microhardness measurements were made on 24 samples treated for 30 min each, with the first sample at 500 MPa, the second at 1 GPa, etc., and with the last sample at 12 GPa. The results are depicted in Fig. 6. It is interesting to note that the microhardness behaviour has a remarkable resemblance to that of the *in situ* resistivity (Fig. 3). Initially there is a sharp fall in microhardness leading to a pressure variation of $(100 \pm 20)\,GPa^{-1}$. (Here microhardness is expressed in Vickers Hardness Number.) Beyond 2 GPa, it appears that there is a small increase in the microhardness. As can be seen from Fig. 6, however, beyond 5 GPa no appreciable change is noticed.

5.4. X-ray diffraction studies

The Debye–Scherrer patterns of AS, PS and CS showed that there were no appreciable changes in the values of the ring diameters. While the patterns for AS and PS show a set of sharp rings, those for CS exhibit broad ones. Fig. 7a represents the intensity of the strongest Debye–Scherrer ring obtained for CS and Fig. 7b is that for CS treated at 2 GPa for 0.5 h. In Fig. 7b, a comparatively smaller FWHM is seen, which indicates that the rings become sharper under pressure. Beyond 2 GPa, however, it was observed that no appreciate decrease in the FWHM could be obtained.

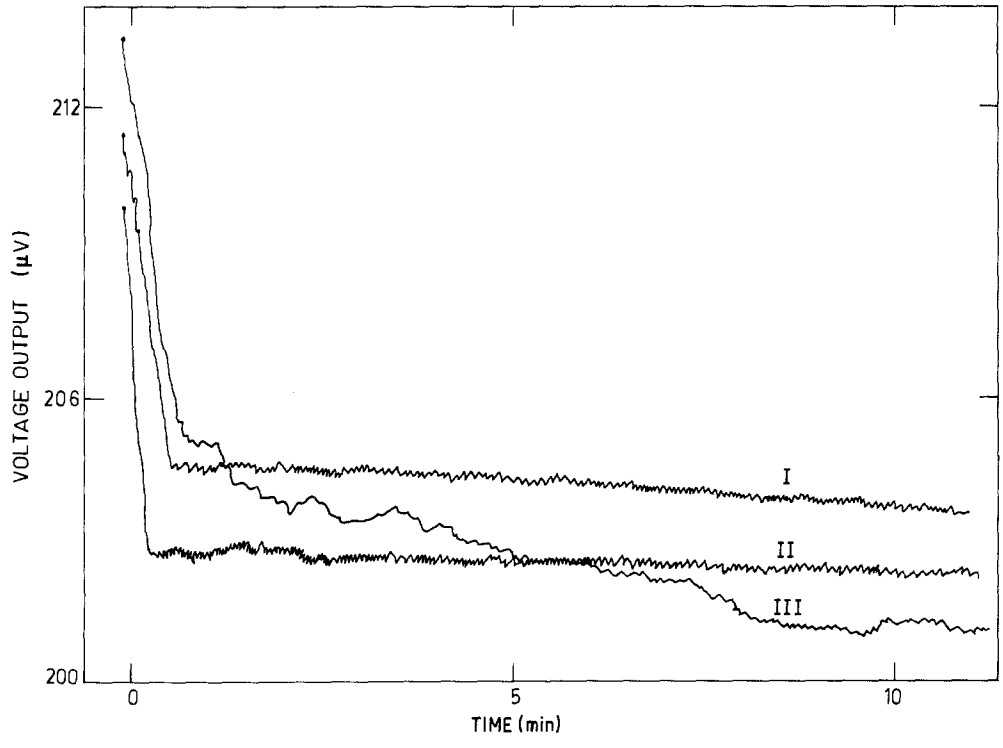

Figure 4 Typical raw data taken with an x–t recorder. The voltage outputs from PS (I) and AS (II) are seen to be weakly time-dependent, and that of the CS (III) exhibits a strong time-dependence. These data were taken at 2 GPa.

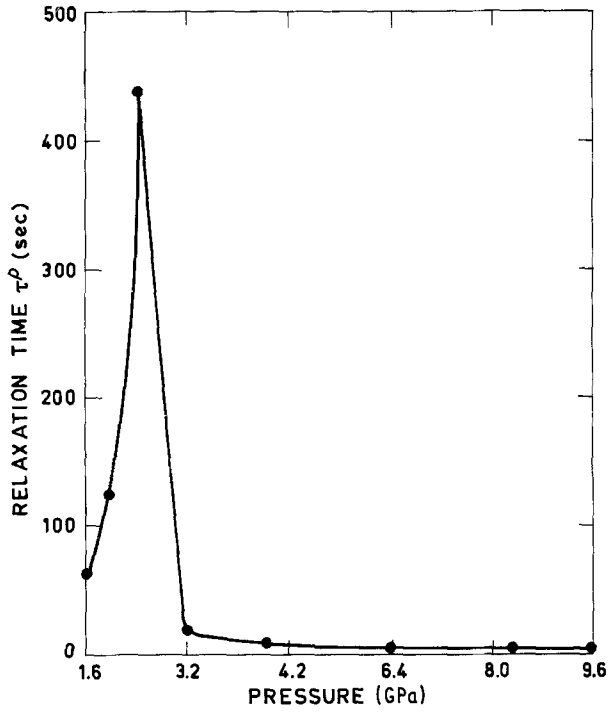

Figure 5 Relaxation time τ^p is plotted as a function of pressure for cold-worked stainless steel. The values are obtained using Equation 7. A maximum at 2 GPa is obtained. Below and beyond 2 GPa, the time-dependence is negligible.

5.5. Transmission electron microscopic studies

Transmission electron micrographs are shown in Fig. 8. Fig. 8a corresponds to the CS sample and Fig. 8b to the CS sample treated at 2 GPa for 30 min. For CS, the dislocations are tangled networks. In contrast, the pressure-treated sample indicates a subgranular or polygonized dislocation structure. It is to be noted that all the samples treated beyond 2 GPa show a polygonized dislocation structure. The dislocation density, D, was calculated using the relation $D = 2NM/Sx$, where N is the number of lines crossing the circle of diameter d, S the circumference (πd) and x the sample thickness. Dislocation densities of CS and CS treated at 20 kbar are $\sim 10^{12}$ and $\sim 10^9 \text{cm}^{-2}$, respectively.

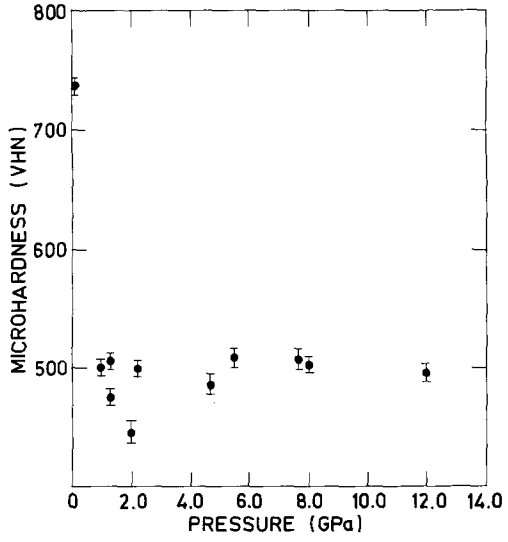

Figure 6 Microhardness data obtained from pressure-quenched samples indicate behaviour similar to that indicated by the *in situ* resistivity shown in Fig. 3.

6. Discussion

The time-dependence of resistivity in CS samples on the application of pressure yields a relaxation time ~ 500 sec at 2 GPa. This is suggestive of the fact that diffusive processes operate, resulting in a time-dependent decrease in $\mathscr{R}$. It is well known that in a severely cold-worked material, a considerable excess concentration of vacancies or interstitials can be achieved. Also in the specific case of stainless steel with a low stacking fault energy (sfe), during deformation, dislocations will be split into partials resulting in a complex arrangement. The observed time-dependent changes can then be attributed to an interaction between the excess point defects and the dislocations, and lead to the annihilation of dislocations or their rearrangement. Since the experiments are done at room temperature where point defects are not normally mobile, the externally applied pressure must in some way aid the point-defect migration. The sign and the magnitude of the activation volume of migration is an indicator of the possibility of defect migration under pressure and its efficiency. Processes with a negative activation volume of migration will be enhanced by pressure.

Calculations of the activation volume of migration in γ-Fe have given a negative value [18, 19] and experiments on molybdenum [1] showed that pressure indeed decreases the Stage III recovery temperature. In the light of these findings, the relaxation effects seen at 2 GPa on CS samples clearly suggest the operation of recovery processes in cold-worked stainless steel.

From the data on self-diffusion [20, 21] for the elements present in stainless steel, the activation energy for self-diffusion is ~ 3.0 eV. A reasonable magnitude for the migration energy can be estimated as ~ 1.0 eV. For 2 GPa pressure, the energy provided to each atom is ~ 0.21 eV. It therefore appears reasonable to assume that the already formed defects will have enhanced migration at 2 GPa. Hence, the recovery is initiated under pressure. However, the observed relaxation time of ~ 500 sec can be explained only after the relevant rate equations for the migration of defects are solved.

The vacancy-aided diffusion process in metals is described by the relation $D = Ga^2 v_0 C_v P_m$ where G, a and v_0 are the geometric factor, the lattice parameter and the Debye frequency, respectively, while C_v and P_m are the probabilities of formation and migration of vacancies in the crystal [22, 23]. To appreciate the effect of pressure on D we should evaluate C_v and P_m, which are given as

$$C_v^p/C_v^0 = \exp(-pV^f/kT) \quad (8)$$

$$P_m^p/P_m^0 = \exp(-pV^m/kT) \quad (9)$$

Here the superscript p stands for pressure and f and m signify the formation and migration mechanisms respectively. Assuming a reasonable value of V^m to be 10% of the atomic volume and its sign to be negative, at 2 GPa, $P_m^2/P_m^0 = 2.3$; that is, the migration

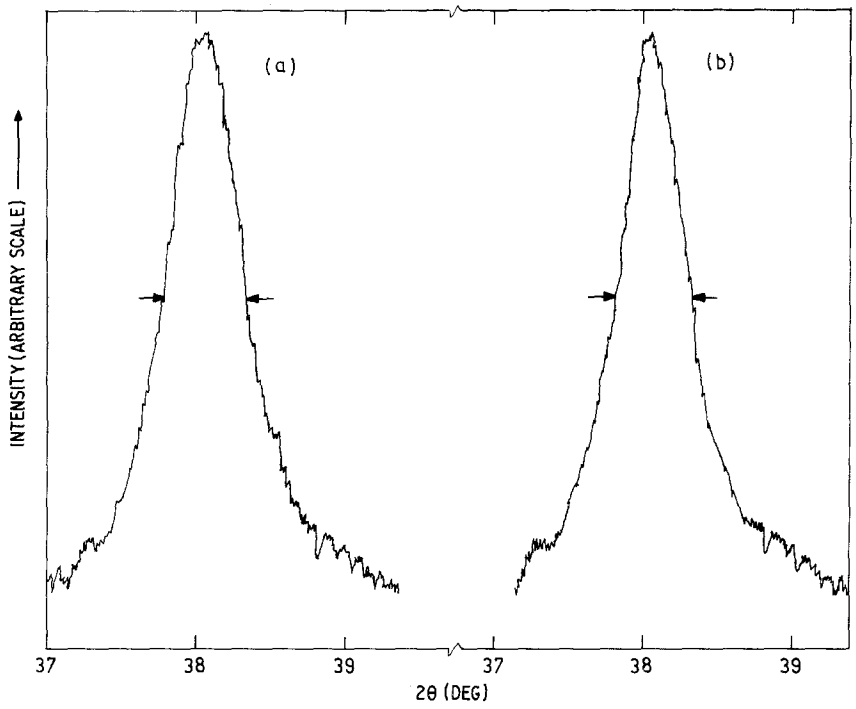

Figure 7 Typical densitometer runs on (a) CS and (b) CS treated at 2 GPa for 30 min. An indication of the decrease in FWHM is obvious in (b).

probability is enhanced by a factor of 2.3. Considering the situation where the already formed vacancies migrate under pressure and are absorbed at the dislocations, a recovery stage at 2 GPa is explicable. For further diffusion to continue beyond 2 GPa, the parameter C_v^f becomes important. This factor, as can be calculated from Equation 8, decreases by four orders of magnitude at 2 GPa. This explains a weak dependence of $\mathscr{R}$ with time for pressures beyond 2 GPa.

Experimentally it has been demonstrated that the dislocations act as excellent sinks for migrating vacancies with an efficiency of nearly unity for high sfe materials, and between 0.5 and 1 for low sfe materials [24, 25]. 316 stainless steel is a low sfe material [26]. It follows that the excess vacancies activated by pressure move to dislocations, which in turn after absorbing the vacancies become mobile. Subsequently, these dislocations can rearrange and annihilate each other as well [27, 28]. The presence of any internal stress has a remarkable effect on these processes [29, 30].

As is well known, polygonization enhances topological ordering at the expense of the orientational coherence between local lattice directions [31]. Why this occurs can be understood from the principles of thermodynamic stability, and how it occurs under pressure can be discussed as follows.

The elastic strain energy about each dislocation stored in the medium is proportional to the logarithm of the area per dislocation. Hence, an increase in the dislocation density will decrease this energy to achieve a stable configuration [31]. On the other hand, the critical stress needed to glide one dislocation past another identical dislocation varies inversely as the distance between the slip planes. With the above two limits defined let us enquire into the possibility of formation of polygonized structure in cold-worked metals such as aluminium and iron, and cold-worked systems under pressure (CS). The stacking fault energy plays a dominant role in polygonization. For example, it occurs very easily in aluminium (high sfe) but is hardly observed in copper (medium sfe). As the absorption efficiency of vacancies is large for high sfe materials, a large number of dislocations are rendered mobile. In zinc, a stress $\sigma \sim 50\,\mathrm{g\,mm^{-2}}$ leads to

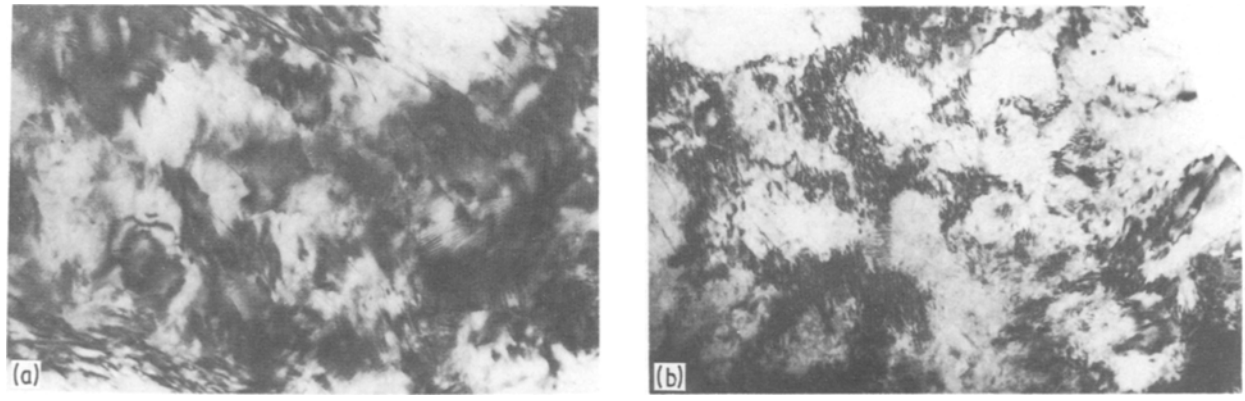

Figure 8 Microstructure of cold-worked stainless steel as observed in the TEM at a magnification of 10^5 (print magnification 8.6×10^4). (a) CS sample indicating a tangled dislocation structure; (b) dislocation structure in CS treated at 2 GPa for 30 min. It is observed that the tangled dislocation structure transforms to a subgranular structure after pressure treatment.

polygonization. Here it is argued that the activation energy of polygonization $U \sim 1.36\,\text{eV}$ is reduced by an amount $\beta\sigma = 0.1\mu b^3 \sim 0.4\,\text{eV}$ for $\sigma \sim 50\,\text{g mm}^{-2}$ [32, 33]. Here μ is the shear modulus, b the Burgers vector and β is a constant.

For stainless steel, a low sfe material, we assume that the activation energy for polygonization is large, $\sim 2\,\text{eV}$ [34, 35]. Here U will include the energy of formation of jogs and vacancies and the migration of the latter. This can be compared with the situation where polygonization in high sfe material is considered. Here the activation energy for polygonization is controlled by the activation energy of migration of vacancies [34, 35]. In cold-worked materials where very large number of vacancies are present and pressure is applied, the diffusion of vacancies is dominated by the activation energy of migration. Consequently, U in cold-worked low sfe material under pressure will be dictated by the energy of formation of jogs plus that of the migration of vacancies.

Under pressure, the yield stress or the mean internal stress increases [36] which can be approximated as

$$\sigma^p = \sigma^0(1 + \alpha p) \qquad (10)$$

Assuming internal stress $\sigma^0 = 0.1\mu \sim 10\,\text{GPa}$ and $\alpha \sim 10^{-1}\,\text{GPa}^{-1}$ for CS [37, 38], at 2 GPa $\sigma^p \sim 12.\text{GPa}$ resulting in the reduction in U by $\sigma^p b^3 = 0.6\,\text{eV}$. Thus the activation energy for polygonization is reduced by the application of pressure and becomes small enough to allow the process to operate.

7. Conclusion

Hydrostatic pressure influences the density and topological disposition of dislocations in a metal. This has been conclusively seen in the present work in which AISI Type 316 stainless steel has been chosen as the test material. Pressure affects the density of dislocations and their rearrangement through the excess concentration of vacancies provided by the high degree of cold work. Pressure enhances their migration probability at 2 GPa by a factor of 2.3. The migrating vacancies are absorbed at dislocation sinks, rendering them mobile. The mobility of dislocations is aided by pressure since the activation energy for a process such as polygonization is reduced by 0.6 eV at 2 GPa.

Acknowledgements

The authors are grateful to Dr G. Venkataraman for his continued interest in this work. They have benefited considerably from discussions and comments from Dr P. Rodriguez. The help of Smt M. Vijayalakshmi in the electron microscopy part of the work is also thankfully acknowledge. It is a pleasure to thank Shri T. D. Sundarakshan, Miss S. Subhashini and the Drawing Office of MSL for their assistance in the preparation of this paper.

References

1. G. L. KULCINSKI, *Phys. Rev.* **179** (1969) 676.
2. T. EGAMI, *J. Mater. Sci.* **13** (1978) 2587.
3. MOHAMMAD YOUSUF and K. GOVINDA RAJAN, *J. Mater. Sci. Lett.* **3** (1984) 149.
4. P. Ch. SAHU, MOHAMMAD YOUSUF and K. GOVINDA RAJAN, in Proceedings of Workshop on Actinides under Pressure, EITU, Karlsruhe, FRG (1983).
5. K. GOVINDA RAJAN, *Curr. Sci.* **53** (1984) 1115.
6. J. M. ZIMAN, in "The Physics of Metals", Vol. 1, edited by J. M. Ziman (Cambridge University Press, Cambridge, 1969) p. 250.
7. P. G. SHEWMON "Transformation in Metals" (McGraw-Hill, New York, 1969) p. 71.
8. J. M. ZIMAN, "Electrons and Phonons" (Clarendon Press, Oxford, 1960) p. 341.
9. *Idem*, "Electrons and Phonons" (Clarendon Press, Oxford, 1960) p. 350.
10. H. WEVER, O. SEYDEL and G. FROHBERG, in "Point Defects and Defect Interactions in Metals", edited by J. Takamura, M. Doyama and M. Kiritani (Tohoku University, Tohoku, 1982) p. 512.
11. V. SEETHARAMAN and R. KRISHNAN, *J. Mater. Sci.* **16** (1981) 523.
12. V. S. SASTRY, R. KHANNA and K. GOVINDA RAJAN, *Rev. Sci. Instrum.* **53** (1982) 1484.
13. Ph. SCHAUFELBERGER, H. MERX and M. CONTRE, *High Temp. High Press.* **5** (1973) 221.
14. C. Y. LIU, K. ISHIZAKI, J. PAAUWE and I. L. SPAIN, *ibid.* **5** (1973) 359.
15. G. L. KINSLAND, *ibid.* **10** (1978) 652.
16. A. K. SINGH, *ibid.* **10** (1978) 641.
17. K. VARATHARAJAN and R. V. NANDEDKAR, *Bull. Electron Micros. Soc. India* **2** (1978) 121.
18. R. A. JOHNSON Jr, *Phys. Rev.* **145** (1966) 423.
19. J. R. BEELER, *ibid.* **150** (1966) 470.
20. V. S. RAGHUNATHAN and B. D. SHARMA, *Phil. Mag.* **43A** (1981) 427.
21. F. H. WOHLBIER (ed.), "Diffusion and Defect Data" Vol. 14 (Trans Tech Publications, Ohio, 1976) p. 47.
22. L. A. GIRIFALCO, "Statistical Physics of Materials," (Wiley, New York, 1973) p. 260.
23. L. A. GIRIFALCO and D. O. WELCH, "Point Defects and Diffusion in Strained Metals" (Gordon and Breach, New York, 1967) p. 32.
24. F. PRING, A. S. ARGON and W. C. MOFFATT, *Acta Metall.* **30** (1982) 821.
25. R. E. SMALLMAN, in "Modern Physical Metallurgy" (Butterworths, London, 1970).
26. P. B. HIRSCH, in "The Physics of Metals", edited by P. B. Hirsch (Cambridge, 1975) Vol. 2.
27. P. G. SHEWMON, "Transformation in Metals" (McGraw-Hill, New York, 1969) p. 71.
28. R. W. CAHN, in Proceedings of the Conference on Dislocations and Properties of Real Materials, Metallurgical Society, London, December 1984 (in press).
29. J. FRIEDEL, in "Physics of Defects", edited by R. Balian, M. Kleman and J. Poirier (North-Holland, Amsterdam, 1981) p. 1.
30. S. V. RAMANI, P. MUKHOPADHYAY, P. RODRIGUEZ and R. KRISHNAN, in "International Symposium on Defect Interactions in Solids", edited by K. I. Vasu, K. S. Raman, D. H. Sastry and Y. V. R. K. Prasad (Indian Institute of Sciences, Bangalore, 1972) p. 346.
31. J. M. ZIMAN, "Models of Disorder" (Cambridge University Press, Cambridge, 1979) p. 53.
32. G. BORELIUS, in Report of 9th Salvay Conference (1952) p. 427.
33. A. H. COTTRELL, "Dislocation and Plastic Flow in Crystals" (Clarendon Press, Oxford, 1963) p. 188.
34. S. S. GORELIK, "Recrystallization in Metals and Alloys" (Mir Publications, Moscow, 1981) p. 86.
35. H. G. VAN BUEREN, "Imperfections in Crystals" (North-Holland, Amsterdam, 1960).
36. A. H. COTTRELL, "Dislocations and Plastic Flow in Crystals" (Clarendon Press, Oxford, 1963) p. 187.
37. R. BULLOUGH, "The Theory of Imperfect Crystalline Solids – Trieste Lectures" (IAEA, Vienna, 1971) p. 143.
38. M. BRANDES, in "Mechanical Behaviour of Materials Under Pressure", edited by H. Le and D. Pugh (Elsevier, London, 1970).

Received 28 May
and accepted 5 August 1985